

Biological Diversity from a Structurally Diverse Library: Systematically Scanning Conformational Space Using a Pyranose Scaffold[†]

Giovanni Abbenante,[‡] Bernd Becker,[‡] Sébastien Blanc,[§] Chris Clark,[‡] Glenn Condie,[‡] Graeme Fraser,[§] Matthias Grathwohl,[‡] Judy Halliday,[‡] Senka Henderson,[‡] Ann Lam,[‡] Ligong Liu,[‡] Maretta Mann,[‡] Craig Muldoon,[‡] Andrew Pearson,[‡] Rajaratnam Premraj,[‡] Tracie Ramsdale,[‡] Tony Rossetti,[‡] Karl Schafer,[‡] Giang Le Thanh,[‡] Gerald Tometzki,[‡] Frank Vari,[‡] Géraldine Verquin,[‡] Jennifer Waanders,[‡] Michael West,[‡] Norbert Wimmer,[‡] Annika Yau,[‡] Johannes Zuegg,[‡] and Wim Meutermans^{*‡}

[‡]*Alchemia Ltd, Eight Mile Plains, Queensland 4113, Australia, and* [§]*Euroscreen SA, Brussels 1070, Belgium*

Received March 2, 2010

Success in discovering bioactive peptide mimetics is often limited by the difficulties in correctly transposing known binding elements of the active peptide onto a small and metabolically more stable scaffold while maintaining bioactivity. Here we describe a scanning approach using a library of pyranose-based peptidomimetics that is structurally diverse in a systematic manner, designed to cover all possible conformations of tripeptide motifs containing two aromatic groups and one positive charge. Structural diversity was achieved by efficient selection of various chemoforms, characterized by a choice of pyranose scaffold of defined chirality and substitution pattern. A systematic scanning library of 490 compounds was thus designed, produced, and screened *in vitro* for activity at the somatostatin (sst_{1–5}) and melanin-concentrating hormone (MCH₁) receptors. Bioactive compounds were found for each target, with specific chemoform preferences identified in each case, which can be used to guide follow-on drug discovery projects without the need for scaffold hopping.

Introduction

For over 20 years new concepts in peptidomimetic chemistry have been developed with the aim of transposing structural and functional requirements for bioactivity from a peptide onto metabolically more stable and drug-like scaffolds.¹

The functional requirements for bioactivity of a peptide are dictated by the nature of the binding elements directly involved in receptor binding (side chains of the amino acid motif and, possibly, backbone elements), while the structural requirements are dictated by the relative orientation of these binding elements (bioactive conformation). With well-defined peptide conformations and motifs, small peptidomimetic molecules can be designed by appending substituents that mimic the binding elements onto a rigid organic scaffold in a way that positions these elements in a similar relative orientation to that in the bioactive peptide conformation. One such example scaffold is the pyranose ring system, pioneered as a peptide mimetic scaffold by the Hirschmann group in the early nineties to mimic a specific set of conformations of the KWF loop of SST14, the somatostatin hormone and endogenous ligand of the sst_{1–5} receptors.^{2–11} A significant body of work has accumulated since using a monosaccharide scaffold in various peptidomimetic design approaches.^{12–19}

However, despite success in the field, the design of bioactive peptide mimetics remains a challenging task. Chemically accessible scaffolds that deliver a seemingly high topographical overlay with the bioactive conformation(s) of the natural ligand do not necessarily deliver the desired activity. This may be further complicated by an inability to accurately predict the bioactive conformation of the peptide. Hence, instead of trying to mimic only specific postulated bioactive conformations, we have aimed to develop a more systematic approach by designing libraries of molecules that, together, comprehensively mimic the possible conformations of the amino acid motifs in the parent peptide. The pyranose scaffold is ideally suited for this purpose because of its unique versatility in terms of positioning three substituents in three-dimensional space (diverse presentations) and the significant overlay of this accessible topographical space with tripeptide conformational space.²⁰

We have been interested in utilizing this unique characteristic of the pyranose scaffold to develop a systematic drug discovery approach toward bioactive peptidomimetics. Our approach involves the production and *in vitro* testing of a library of pyranose-based mimetics where the 3D presentation, defined by the order and positioning of the three highlighted vectors in Figure 1, is systematically varied to cover the range of topographies accessible to tripeptides, thereby effectively scanning for peptidomimetics with the desired bioactivity profile. To avoid misunderstandings of the word “presentation” we have coined the term “chemoform” to specifically describe the order and positioning of the three vectors. The premise of our approach is that each receptor will have a chemoform

[†]In memory of our colleague, Gerry Tometzki.

^{*}To whom correspondence should be addressed. Phone: 61-7 3340 0200. Fax: 61-7 3340 0222. E-mail: wmeutermans@alchemia.com.au. Website: www.alchemia.com.au.

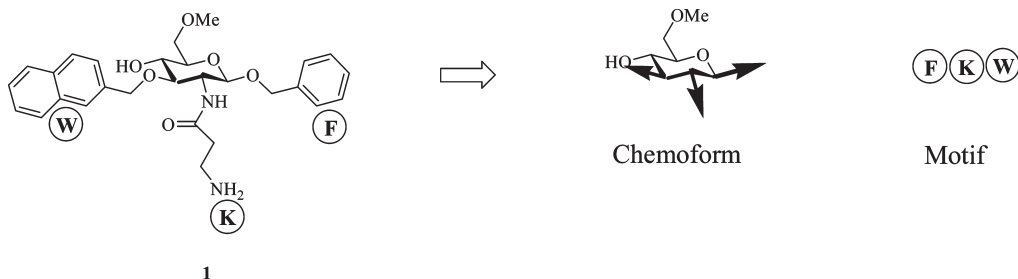


Figure 1. Break down of a pyranose-based peptidomimetic in terms of chemoform and motif.

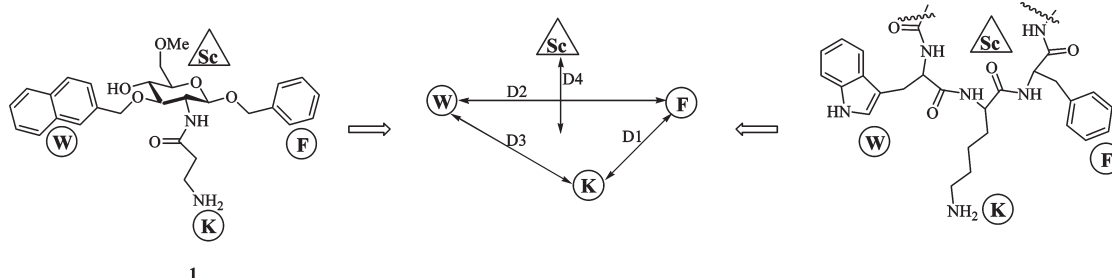


Figure 2. An example pyranose-based mimetic of the FKW tripeptide motif and the four distances that are determined from a calculated low energy conformation to describe the presentation. F = phenylalanine mimetic; K = lysine mimetic; W = tryptophan mimetic; Sc = scaffold; D1 = distance between F and K; D2 = distance between F and W; D3 = distance between W and K; D4 = distance from scaffold center perpendicular to the FKW plane.

preference that, once defined, can be used as a basis in structure–activity relationship (SAR⁴) design to move from hit-to-lead and beyond, without the need for scaffold hopping.

Here we describe the design, production, and biological evaluation of a systematic structurally diverse library around a tripeptide motif containing two aromatics and one positive charge. The molecular shape is varied by selecting chemoforms that are different from each other and synthetically feasible through the same synthetic strategy. This systematic scanning library was screened against the somatostatin receptor subtypes (sst_{1–5}) and the melanin-concentrating hormone receptor 1 (MCH₁), examples of class A G-protein coupled receptors (GPCR) known to bind peptides containing this tripeptide motif, and actives analyzed to define unique chemoform and motif preferences for each selected receptor.

Results

Design of a Pyranose-Based FKW Scanning Library. Central to the scanning concept is the selection of compounds to be included in the library. The design of our scanning library follows three basic principles:

- 1 Comprehensive: The library needs to include a range of chemoforms in order to cover the tripeptide conformational space comprehensively.
- 2 Systematic—compound efficient: The compounds included in the library need to cover that tripeptide conformational space evenly.

- 3 Minimal synthetic effort: All compounds in the library should be accessed from common building blocks to simplify the synthetic effort required for the library production.

The design of the pyranose library and its comparison with peptides was done using the three side chains from the FKW tripeptide motif (phenylalanine, lysine, and tryptophan) as the reference model. The set of pyranose presentations selected for this FKW conformational scanning library were then used for all motifs containing two aromatics and one positive charge.

Distances between the key features of the compounds have been used as descriptors of 3D shape for each compound (Figure 2). The key features include the mass center of the binding elements on each substituent, and the mass center of the scaffold, as outlined in Figure 2. Four distances have been included in the list of descriptors: three distances between each of the three different substituents (between F–K, K–W, and W–F) and one distance between the scaffold (Sc) and the plane spanned by the three substituents (F, K, and W). This latter descriptor defines the relative position of the scaffold to the FKW plane, i.e., the sign (\pm) of the distance, calculated using a fixed order for the plane definition (F, K, W) and the right-hand rule, defines the scaffold position as either above or below the plane. This descriptor is thereby able to describe the chirality of the molecule. Furthermore, the same descriptors can easily be generated for a tripeptide, using the mass center of the peptide backbone atoms as scaffold (Sc). Compound or tripeptide conformations can now be compared and similarity/dissimilarity calculated by the Euclidian mean of the differences in their four distances.

For the design of our scanning library, we need to first define the conformational tripeptide space that we wish to cover. For this purpose, we extracted all tripeptide fragments containing F, K, or W, in any order, from a set of NMR and X-ray structures with less than 25% sequence identity (Pdb_Select_25) to each other.²¹ A total of 259 FKW tripeptide

⁴ Abbreviations: C, chemoform; CG, chemoform group; Cpd, compounds; DIPEA, *N,N*-diisopropylethylamine; DMPFN, 3,5-dimethyl-1-pyrazolylformamidinium nitrate; DTT, dithiothreitol; EDTA, ethylenediaminetetraacetic acid; GPCR, G-protein coupled receptor; HBTU, *O*-Benzotriazole-*N,N,N',N'*-tetramethyl-uronium-hexafluorophosphate; MCH, melanin-concentrating hormone; PDB, Protein Data Bank; Pip, piperidine; PSHF, proton sponge HF; QC, quality control; RLB, radioligand binding; rmsd, root-mean-square deviation; SAR, structure–activity relationship; Sc, scaffold; sst, somatostatin; TBDPS, *tert*-butyldiphenylsilyl; TES, triethylsilane; TFA, trifluoroacetic acid.

fragments were extracted and the corresponding four distance descriptors calculated from the coordinates as found in their corresponding X-ray or NMR structure. Figure 3 shows the 259 FKW tripeptide conformations in a two-diagram plot, D1–D2 and D3–D4.

The distances between the side chain substituents range from 4 to 16 Å for D1–D3, whereas the distance of the backbone to the plane (D4) ranges from –5 to +5 Å.

To evaluate the level of rigidity of the pyranose-based mimetics, a conformational analysis was carried out on the example molecule **1** in Figure 1. This included systematic variation of the pyranose ring conformation and of the first rotatable torsional angle of each substituent followed by energy minimization. Conformations with energy greater than 5 kcal from the lowest energy conformation were discarded. In addition, only low energy conformations with root-mean-square deviation (rmsd) of heavy atom positions greater than 1 Å were selected for the conformational flexibility analysis, resulting in a diverse set of low energy conformations.

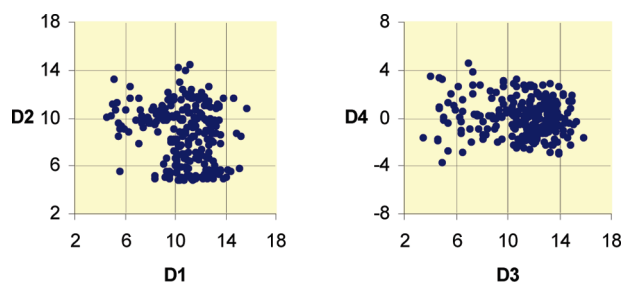


Figure 3. Distances D1–D4 (expressed in two diagrams, D1–D2 and D3–D4) for FKW tripeptide sequences found in crystal structures of proteins, obtained from the Protein Data Bank (PDB). All distances are in Å.

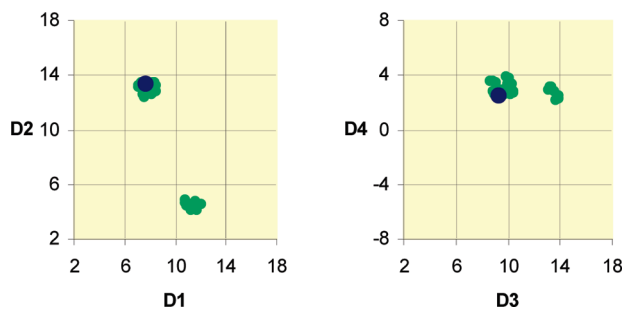


Figure 4. Distances D1–D4 for low energy conformations of compound **1**. Dark-blue solid circles: A single calculated low energy conformation used as starting point for the conformational analysis. Green solid circles: Multiple low energy conformations of compound **1** within 5 kcal, obtained from conformational analysis. All distances are in Å.

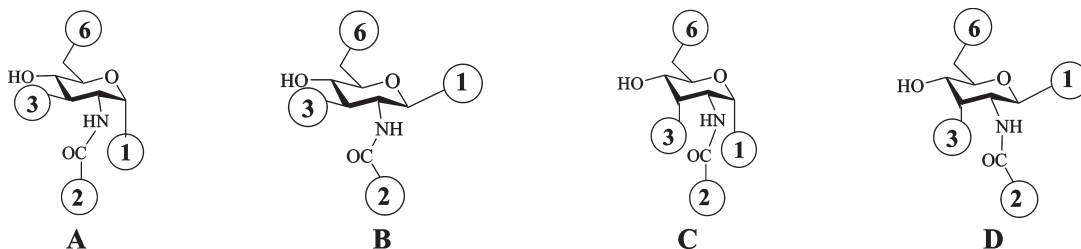


Figure 5. General structures for the four scaffolds (Sc) from which the scanning library was designed and built: (A) α -D-glucosamine, (B) β -D-glucosamine, (C) α -D-allosamine, and (D) β -D-allosamine.

The results of the conformation analysis can be visualized by plotting the four distances in a two diagram plot. The single low energy conformation of the glucose-based FKW mimetic **1** is marked in dark blue, and the remaining low energy conformations in green. Figure 4 clearly shows two clusters of conformations for the example FKW-mimetic.

In what follows, only one low energy conformation is plotted out for each mimetic. The main purpose of this analysis is to help define the area in the diagrams populated by the FKW tripeptide motif and guide the design of our diversity library.

In the design of a pyranose-based scanning library, consideration must also be given to the synthetic feasibility and implementation of the library assembly process. We have previously described a solid phase synthetic approach using allose- and glucose-based scaffolds for the parallel production of pyranose-based mimetics.²² Having established this versatile and regiospecific synthetic route, we wanted to design a FKW-scanning library based on the glucose and allose scaffolds A–D (Figure 5).

This synthetic route includes resin linkage at position 4 of the scaffolds, leaving four positions available to attach the three side-chain mimetics (from the FKW tripeptide), leading in principle to 24 possible chemoforms per scaffold, or a total of 96 chemoforms. To simplify the library production, only amine substituents were considered at position 2, which brings the number of chemoforms to six per scaffold. On the basis of a simple vector overlay analysis revealing similarities between chemoforms, the number of chemoforms included for the production of our scanning library was further reduced to the 16 chemoforms listed in Table 1. For each of these chemoforms, a combinatorial library of 6–9 compounds was then created by combining up to three substituents for each amino acid (3 lysine, 2–3 phenylalanine (depending on the position of F), and 1 tryptophan mimetics, see Table 2). This results in a scanning library of 114 compounds, to mimic the FKW tripeptide motif in various spatial orientations.

To evaluate the extent of overlap of this library with the FKW tripeptide conformational space described in Figure 3, the four distance descriptors were calculated for each of the 114 mimetics using one low energy conformation per mimetic. The distance plots in Figure 6 show that the distances D1–D3 ranged from 4 to 16 Å and D4 ranged from –6 to +6 Å, i.e., the D1–D4 values for the FKW tripeptide fragments (Figure 3) fall within the range covered by the pyranose-based mimetics. In addition, the plot illustrates that the mimetics in this scanning library are spread across this range.

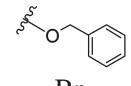
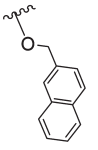
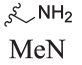
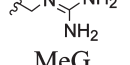
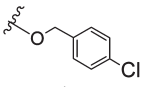
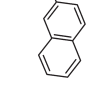
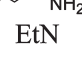
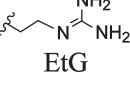
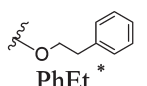
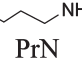
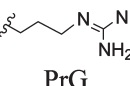
Thus far we have described the design of a FKW mimetic library. For this study, we wanted to apply the concept of structurally diverse pyranose-based peptide mimetics to the general aromatic–aromatic–positive charge motif, including

Table 1. Chemoforms Selected for the Scanning Library

C ^a	Sc (Figure 5)	position on scaffold				no. of Cpds
		1	2	3	6	
1	A	F	K	W	OMe	9
2	A	W	K	F	OMe	6
3	B	F	K	W	OMe	9
4	B	W	K	F	OMe	6
5	C	F	K	W	OMe	9
6	C	W	K	F	OMe	6
7	D	F	K	W	OMe	9
8	D	W	K	F	OMe	6
9	A	F	K	OMe	W	9
10	A	W	K	OMe	F	6
11	B	F	K	OMe	W	9
12	B	W	K	OMe	F	6
13	B	SMe	K	F	W	6
14	B	SMe	K	W	F	6
15	D	SMe	K	F	W	6
16	D	SMe	K	W	F	6

^a Chemoforms (C) are defined as combinations of scaffold and substitution pattern; Scaffolds (Sc) are defined as depicted in Figure 5: (A) α -D-glucosamine; (B) β -D-glucosamine; (C) α -D-allosamine, and (D) β -D-allosamine.

Table 2. Definition of the Substituents Used in the Design of the Scanning Library to Mimic Amino Acid Side Chains^a

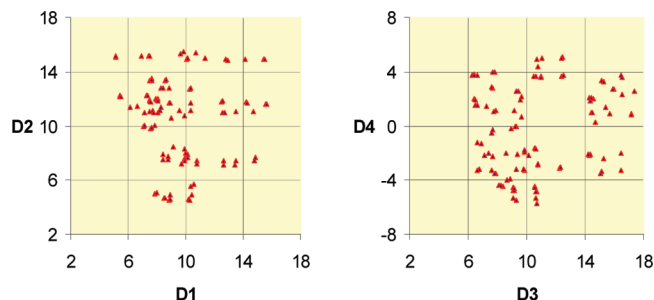
Aromatics (Positions 1,3,6)		Positively charged (Position 2)	
Phe (F)	Trp (W)	Lys (K)	Arg (R)
			
			
			

^a *Only used at position 1 of the scaffolds.

peptide motifs such as FKF and WKW, as well as extending the motif with an arginine mimetic, FRW, FRF, and WRW. For these additional motifs, the same list of chemoforms in Table 1 and substituents described in Table 2 for F, W, K, and R were included in the library design.

The resulting designed library contains 540 compounds and is effectively a combinatorial library of the aromatic–aromatic–positive charge motif across eight chemoforms (note that due to the symmetry in the aromatic–aromatic–positive charge motif, the number of chemoforms in Table 1 is halved, as C1=C2, C3=C4, etc.).

Production of the Library. The general synthetic route has been described elsewhere and is summarized in Scheme 1. Although the synthetic route will deliver anomerically pure single compounds from anomerically pure glycosides, the preference in this library production was given to synthesize α/β anomeric mixtures in order to reduce the production and purification efforts and the in vitro screening costs. Once hits are identified from screening this library, they are resynthesized as individual anomers and retested. For this reason, in our library description (Table 3), we have grouped chemoforms together in chemoform groups (CG I–V). Screening

**Figure 6.** Distances D1–D4 for 114 pyranose-based FKW mimetics in Table 1. All distances are in Å.

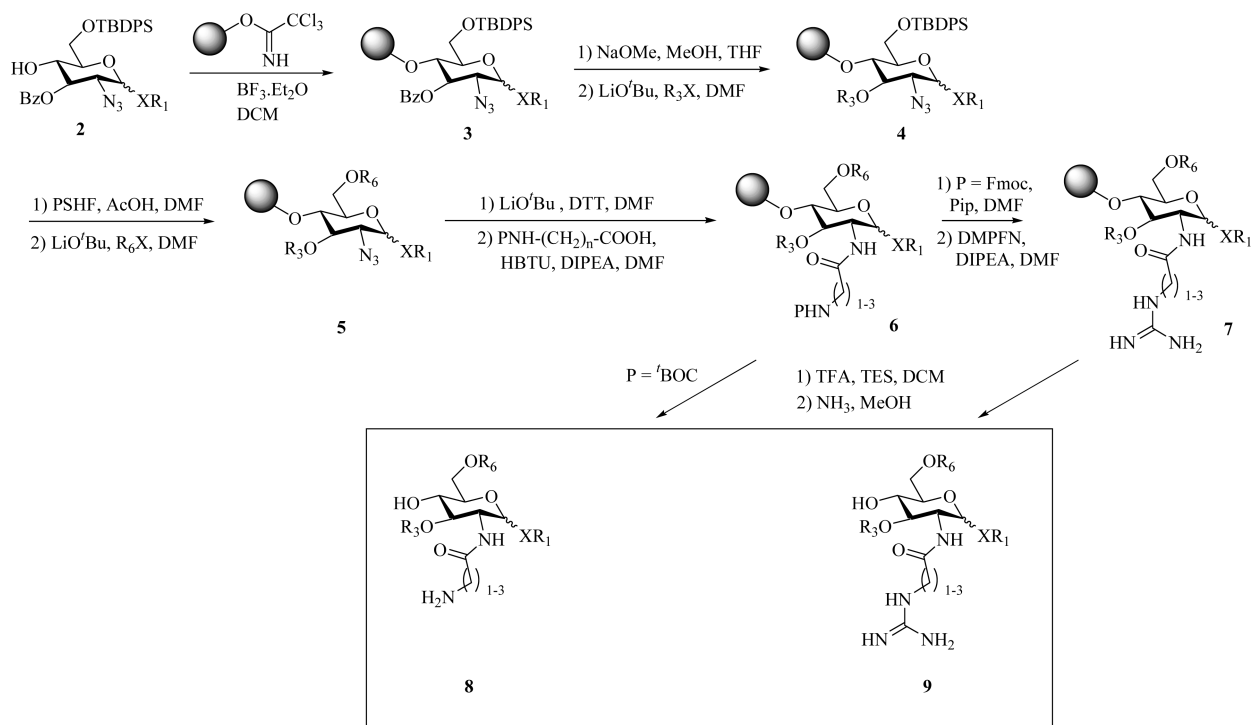
of the library will initially provide information on active chemoform groups, and resynthesis and retesting of hits will help define active chemoforms.

We used the synthetic route in Scheme 1 starting from α/β mixtures of glycosides **2** (either allose or glucose configuration), obtained from glycosylation of the corresponding thiomethyl glycosides.²³ Conditions of glycosylation were optimized to obtain between 1/3 and 1/1 α/β anomeric ratio as determined by NMR analysis. The α/β glycoside mixtures and β -thiomethyl-glycoside building blocks were loaded on the resin and resins **3** carried through the synthetic process²² using Irori mini-Kan technology in a split-and-mix library approach.²⁴ In brief, the benzoate protecting group was removed using Zemplén conditions and alkylation performed using LiO^tBu and an alkyl bromide to generate intermediate **4**. Treatment with the HF salt of proton sponge removed the *tert*-butyldiphenylsilyl (TBDPS) protecting group at 6, and alkylation, performed as before, introduced the substituent at position 6. Reduction of the azide **5** with dithiothreitol (DTT), followed by acylation using *O*-benzotriazole-*N,N,N',N'*-tetramethyl-uronium-hexafluoro-phosphate (HBTU) activation, afforded the protected amine **6**. To afford the amine-based mimetics **8**, BOC amino acids were used in the previous step, followed by TFA induced cleave-deprotection. To produce the guanidine-based mimetics **9**, the resin-loaded free amine was guanylated using 3,5-dimethyl-1-pyrazolyl-formamidinium nitrate (DMPFN) prior to cleavage from resin.

All products were isolated by HPLC to generate pure samples for in vitro testing (either α/β mixtures or pure anomers). Table 3 summarizes the number of compounds designed and successfully obtained per chemoform group, with an average purity of 97% as measured by ELSD.

Screening for Activity at the sst_{1–5} Receptors. Somatostatins are a family of cyclopeptides that bind to the G-protein-coupled receptor subtypes sst_{1–5} and act as potent inhibitors of various endocrine (growth hormone, insulin, glucagon, gastrin, cholecystokinin, vasoactive intestinal polypeptide, secretin) and exocrine (gastric acid, pancreatic enzymes) secretory processes, as well as modulation of cell proliferation.^{25–30} Critical for receptor recognition are the β -turn amino acids tryptophan and lysine, and this has formed the basis for the design and development of several metabolically stable peptide analogues as well as many glucose-based turn mimetics from the Hirschmann laboratories in the past two decades.^{2,3,5,6,8}

Our library, scanning the FKW motif, was initially screened for radioligand binding (RLB) activity at the sst_{1–5} receptors using aequorin cell lines for each of human sst_{1–5} receptors. The bias in the library design yielded a high hit rate. A number of top actives were selected based on the single point

Scheme 1. Synthetic Route towards the Pyranose-Based Mimetics in the Designed Scanning Library**Table 3.** Chemoform Groups (CG) Included in the Synthetic Library Scanning the Aromatic–Aromatic–Positive Charge Motif

CG	C (Table 1)	Sc (Figure 5)	position on scaffold				no. of Cpds		success rate (%)	no. of samples ^b
			1	2	3	6	designed	obtained ^a		
I	1–4	A/B	Ar	Pos	Ar	OMe	144	124	92	62
II	5–8	C/D	Ar	Pos	Ar	OMe	144	144	100	72
III	9–12	A/B	Ar	Pos	OMe	Ar	144	138	96	69
IV	13,14	B	SMe	Pos	Ar	Ar	54	30	56	30
V	15,16	D	SMe	Pos	Ar	Ar	54	54	100	54
total							540	490	92	287

^a Definition of synthetic success was based on LCMS analysis (correct MW and > 80% purity of the combined α/β products by ELSD), and on weight of material obtained after purification (> 1 mg). ^b Number of samples (single compound and α/β mixtures) tested. The synthesis delivered 490 compounds from 540 designed compounds in 287 samples (for group I–III all compounds are initially tested as α/β mixtures).

screening for each of the sst_{1-5} receptors for confirmatory IC_{50} determination.

Table 4 lists the structures and IC_{50} of the five top hits for the sst_4 and sst_5 receptors from this confirmatory screening. The top sst_4 hits share the same substitution pattern and scaffold, indicating that the sst_4 receptor binds preferentially to molecules of this chemoform group (CG V) over the other chemoform groups in the library. In addition, the sst_4 receptor tolerates guanidines and amines in the binding motif. The sst_5 top hits also share a common substitution pattern but with no specific chiral center preference (CG I and II). These sst_4 and sst_5 binding chemoforms are clearly distinct as visualized in Table 4.

The top hits for the sst_{1-3} receptors were analyzed following the same principles. Table 5 lists the affinity range and the structural features of the top 5 confirmed hits for the sst_{1-5} receptors. Submicromolar hits were identified for the sst_{2-5} receptors.

For selected sst_5 hits from groups I and II, the individual anomers were synthesized for confirmatory testing and evaluation of subtype selectivity. Table 6 summarizes RLB IC_{50} results across sst_{1-5} for single stereoisomers. The sst_5 actives show good selectivity over sst_4 and vice versa, as would be

expected from the chemoform analysis in Table 4. The sst_5 receptor does not appear to have a clear preference for one anomer over the other. All compounds in the table have agonist or partial agonist activity.

Screening for MCH₁ Receptor Antagonists. Melanin-concentrating hormone is a 19 residue cyclic peptide that binds with high affinity to two receptors, MCH₁ and MCH₂, with pharmacological activity in body weight regulation.^{31–38} MCH₁ antagonists have been demonstrated to reduce weight in rodents^{39,40} and are being pursued for the development of novel antiobesity therapies.^{41–45} Among the MCH residues important for binding are arginine-6,11, tyrosine-13, and tryptophan-17, and MCH₁ small molecule antagonists typically contain aromatics and a basic amine.⁴⁶ As our library is designed to scan the aromatic–aromatic–positive charge motif, we decided to screen this library for antagonist activity at the MCH₁ receptor in a collaborative effort with Euroscreen SA.

Primary screening identified 17 hits (> 50% inhibition at 6.6 μ M in MCH₁ aequorin cell line) from 287 samples in the library. These antagonists were further evaluated in RLB for IC_{50} determination, with seven samples showing binding IC_{50} more potent than 10 μ M. All the confirmed hits, listed in

Table 4. Structures of the Five Top Hits for the sst₄ and sst₅ Receptor

sst₄ preferred chemoform

* Green = aromatic; Blue = positive charge

sst₅ preferred chemoforms

cpd	Sc	Substituents			sst ₄
		2	3	6	IC ₅₀ (μM)
9a	D	EtG	Nap	Bn	0.18
8a	D	EtN	Nap	ClBn	0.43
8b	D	EtN	Nap	Nap	0.44
8c	D	EtN	Nap	Bn	0.66
9b	D	PrG	Nap	ClBn	0.72

cpd	Sc	Substituents			sst ₅
		1	2	3	IC ₅₀ (μM)
8d	A/B	Nap	PrN	ClBn	0.07
8e	C/D	Nap	EtN	Nap	0.10
8f	C/D	Nap	EtN	Bn	0.16
8g	C/D	PhEt	EtN	Nap	0.16
8h	A/B	PhEt	PrN	Nap	0.20

Table 5. Structural Features of Confirmed sst₁₋₅ Hits

target	no. of hits < 10 μM	IC ₅₀ (μM) range of top 5	structural features of top 5	
			CG	Pos ^a
sst ₁	16	1.70–3.30	II	K,R
sst ₂	18	0.65–1.46	II,V	K
sst ₃	15	0.14–0.22	II	K,R
sst ₄	17	0.18–0.72	V	K,R
sst ₅	20	0.07–0.2	I, II	K

^aPos = positive charge, amine (K) or guanidine (R).

Table 7, belong to the same chemoform group I with the common feature of guanidine as the positive charge.

The top five α/β mixtures were resynthesized as individual α or β products and retested. The RLB data demonstrated a consistent preference for the α anomer products over the β isomers, with the best IC₅₀ from the initial hit finding library at 120 nM. Similar to the sst₄ receptor, the MCH₁ receptor preferentially binds to one chemoform, and, as is the case for its peptide ligands, with a preference for guanidine over amine in the binding motif (Table 8).

Discussion

Our interest is in developing a systematic approach toward identifying suitable topographies, i.e., molecular shapes that complement the binding site of the selected target. Our premise is that the pyranose scaffold is a versatile tool to generate diverse molecular shapes that can simulate a broad spectrum of tripeptide conformations. The molecular design principles we have used (measuring four distances for one low-energy conformation) to evaluate this are not sophisticated, as no consideration of the molecular flexibility is made nor consideration of the orientation of the substituent. Figure 4 illustrates the level of flexibility of these types of mimetics, suggesting that each single point (one for each mimetic) in Figure 6 should be seen as a larger sphere of conformations around that point. We have opted to show single conformation per

mimetic in figure 6 to clarify two points: (i) the diagrams in Figures 3 and 6 show good similarity, in terms of the range of distances D1–D4 that are covered by the peptides and the mimetics respectively (4–16 Å for D1–D3 and –4 to +4 Å for D4), (ii) the mimetics in Figure 6 are spread across this D1–D4 accessible tripeptide space. Given that each point in Figure 6 should be considered as covering a larger sphere due to inherent conformational flexibility, we conclude that this library of selected mimetics, although built from a single scaffold, covers the range of accessible tripeptide conformations in terms of positioning the amino acid side chains in space.

The selected motifs for the described library are binding motifs for the sst₁₋₅ and MCH₁ receptors. The screening of this library for activity at these receptors is therefore largely a biological evaluation of the structural diversity in the library. If the library is comprehensive in covering tripeptide conformations, we expect to find active and inactive molecules in the library. This is the case for sst₁₋₅ and MCH₁. In addition to this, the results for both sst₁₋₅ and for MCH₁ screening show that each receptor has a high degree of preference for specific chemoforms or chemoform types in the library. In the case of sst₄, the top actives share a single chemoform, which is distinct from the single chemoform shared by the MCH₁ top actives or the chemoforms recognized by sst₅. For the sst₅ receptor, some chemoform degeneracy can be observed that relates to chiral center inversion, however the general substitution pattern is the same for all sst₅ hits.

Affinity and selectivity are further dictated by the nature of the substituents, as can be observed for the sst₅ and MCH₁ hits. The top hits for both receptors share the same chemoform (C1–2), but the MCH₁ receptor has a preference for guanidine over primary amine whereas the opposite is true for the sst₅ receptor.

This chemoform and motif preference can be visualized in a heatmap (Figure 7), where the library is represented as a matrix of chemoforms (eight for Ar–Ar–Pos motif) and type of positive charge (amine or guanidine), creating 16 wells. By coloring various wells in the heatmap, the top actives per

Table 6. sst₁₋₅ Receptor Binding Affinities for Selected Anomerically Pure Compounds

Cpd	position on scaffold				CG	Sc	IC ₅₀ (μM)				
	1	2	3	6			sst ₁	sst ₂	sst ₃	sst ₄	sst ₅
8d-α	Nap	PrN	ClBn	Me	I	A	>10	>10	0.50	>10	0.07
8d-β	Nap	PrN	ClBn	Me	I	B	>10	>10	0.43	>10	0.05
8h-α	PhEt	PrN	Nap	Me	I	A	>10	6.10	8.40	>10	0.20
8h-β	PhEt	PrN	Nap	Me	I	B	>10	3.32	1.32	>10	0.18
8e-β	Nap	EtN	Nap	Me	II	D	2.80	0.65	0.38	4.00	0.02
8a	SMe	EtN	Nap	ClBn	V	D	9.59	0.98	6.33	0.43	6.00

Table 7. Radioligand Binding Affinities for Selected Hits at the MCH₁ Receptor

Cpd	Sc	position on scaffold			K _i (μM)
		1	2	3	
9c	A/B	ClBn	PrG	ClBn	1.2
9d	A/B	Nap	PrG	ClBn	1.8
9e	A/B	ClBn	PrG	Nap	2.6
9f	A/B	EtPh	PrG	ClBn	3.5
9g	A/B	Nap	PrG	Nap	5.1
9h	A/B	Nap	EtG	Nap	6.3
9i	A/B	Nap	MeG	ClBn	6.6

Table 8. Radioligand Binding Affinities of Single Anomers at the MCH₁ Receptor

Cpd	position						MCH ₁ IC ₅₀ (μM)
	1	2	3	6	CG	Sc	
9c-α	ClBn	PrG	ClBn	Me	I	A	0.12
9c-β	ClBn	PrG	ClBn	Me	I	B	1.66
9d-α	Nap	PrG	ClBn	Me	I	A	0.92
9d-β	Nap	PrG	ClBn	Me	I	B	1.75
9e-α	ClBn	PrG	Nap	Me	I	A	0.45
9e-β	ClBn	PrG	Nap	Me	I	B	>3 ^a
9f-α	PhEt	PrG	ClBn	Me	I	A	0.54
9g-α	Nap	PrG	Nap	Me	I	A	1.16

^aCompound showed < 50% RLB displacement at 3 μM.

receptor can be easily visualized relative to the chemoform selection in the library.

The screening of this “shape” scanning library delivered submicromolar hits for five out of six receptors, from a single library of 490 compounds. The same library was also screened for other receptors recognizing the Ar–Ar–Pos motif, such as melanocortin (MC₁, MC₄) and nociceptin (NOP) receptors (data not shown). Orthosteric hits were identified for all three receptors, and a clear chemoform preference could be associated with each receptor. This high success rate is a reflection of the systematic nature of the library design. By being systematic, we avoid the need to predict bioactive conformation for peptide mimetic design and empirically scan for the bioactive peptide mimetic. As these hits are built on a rigid small molecule scaffold, the consequent hit-to-lead and lead optimization processes may only require alterations at the substituent sites, such as incorporation of more drug-like substituents, without a need to move away from the scaffold, or indeed chemoform, and associated starting materials and chemistries.

We have biased the described library toward specific motifs, targeting selected receptors. We have now assembled a 14000 compound library that is systematically diverse in motif and in chemoform, built on the pyranose scaffold. The screening of this library across many classes of targets will provide further evaluation of the broad applicability of this scanning approach and may provide alternative drug discovery opportunities

for challenging targets where traditional library screening efforts have failed to deliver suitable hits.

Experimental Section

Radioligand Binding Assays on Somatostatin Receptors. Competition binding assays were performed using membranes prepared from CHO cells stably and selectively expressing the cloned, human sst₁, sst₂, sst₃, sst₄, or sst₅ receptors. Assays were carried out in 96-well plates (Master Block, Greiner, 786201) following successive addition of 50 μL of assay buffer (25 mM Hepes pH 7.4, 5 mM MgCl₂, 1 mM CaCl₂, 10 μg/mL Saponin, 0.5% protease free BSA), 10 μL of test compound or reference ligand (Somatostatin-28, Peninsula, 8004), 20 μL of membrane extracts (sst₁ = 2, sst₂ = 0.2, sst₃, sst₄, sst₅ = 0.7 μg protein/well), and 20 μL of radioligand (3-[¹²⁵I] iodotyrosyl¹¹Somatostatin-14, Amersham, IM161). The final concentration of 3-[¹²⁵I] iodotyrosyl¹¹Somatostatin-14 in the assay ranged from 0.07 to 0.42 nM across the receptor subtypes tested. The plate was incubated 60 min at 25 °C in a water bath and then filtered over GF/B filters (Perkin-Elmer, 6005177, presoaked in 0.5% PEI for 2 h at room temperature) with a Filtration unit (Perkin-Elmer). The filters were washed six times with 0.5 mL of ice-cold wash buffer (25 mM HEPES pH 7.4, 5 mM MgCl₂, 1 mM CaCl₂), then 50 μL of Microscint 20 (Packard) was added and the plate was incubated for 15 min on an orbital shaker and then counted with a TopCount for 1 min/well. All values were corrected for nonspecific binding determined by addition of an excess of SST28 (1 μM). K_i values were calculated by nonlinear regression analysis using a single-site model (XLfit, IDBS Software), and the previously determined K_d value of SST28 for the radioligand at each receptor subtype. Compounds were tested once in duplicate samples.

SPA Binding Assays on MCH₁ Receptors. Competition binding assays were performed using membranes prepared from CHO cells stably and selectively expressing the cloned, human MCH₁ receptor. The assay was carried out in an Optiplate (Perkin-Elmer, 60052) wherein test compound (50 μL, used at increasing concentrations) was combined with successive additions of 25 μL of radioligand ([¹²⁵I]-MCH, Perkin-Elmer, NEX 375, 2200 Ci/mMol) diluted in assay buffer (25 mM HEPES pH 7.4, 1 mM CaCl₂, 5 mM MgCl₂, 0.2% protease free BSA) and 25 μL of a premix of membrane/beads (PVT-WGA beads, Amersham, RPNQ0001, 0.25 mg/well). Plates were incubated at room temperature for 2 h before counting for 1 min/well in a TopCount (Packard). Phe-(D)-Tyr-MCH (Bachem, H-2218) was used as the reference ligand. IC₅₀ values were calculated by nonlinear regression analysis using a sigmoidal dose–response model (XLfit, IDBS Software).

AequoScreen Functional Studies on Somatostatin and MCH₁ Receptors. AequoScreen is an aequorin-based assay performed by Euroscreen SA. Assays were performed in CHO cells stably and selectively expressing the cloned, human sst₁, sst₂, sst₃, sst₄, or sst₅ receptors or CHO cells stably and selectively expressing the MCH₁ receptor. Cells in midlog phase, grown in media without antibiotic 18 h prior to the test, were detached by gentle flushing with PBS-EDTA (5 mM EDTA), recovered by centrifugation and resuspended in “BSA medium” (DMEM/HAM’s F12 Gibco cat. no. 11039-021, with HEPES, without phenol red

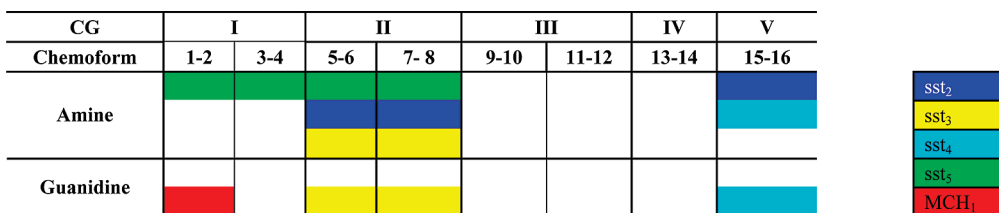


Figure 7. Heatmap of the diversity library highlights the specific chemoform and charge preference for the selected GPCRs.

+0.1% BSA). Cells were then counted, centrifuged, and resuspended in a 15 mL Falcon tube at a concentration of 1.7×10^6 cells/mL. Coelenterazine h (Promega, cat. no. X300X, stock solution: 500 μ M in methanol) was added to the cells in suspension at a final concentration of 5 μ M. The Falcon tube, wrapped in aluminum foil, was then placed on a vertical rotating wheel (6 rpm) and incubated at room temperature (temperature should be maintained below 22 $^{\circ}$ C) overnight in order to reconstitute active aequorin. Cells were counted, diluted in “BSA-medium”, and incubated for 60 min prior to experimentation. For sst receptors, compounds to be tested and reference ligands were diluted in “BSA-medium” and distributed in a 96-well plate (50 μ L/well) prior to injection of cells (5000 cells/50 μ L). For MCH₁ receptor, test and reference compounds were similarly prepared and distributed in a 384-well plate (30 μ L/well) prior to injection of cells (5000 cells/30 μ L). Cells were injected and agonist activity was measured by recording the emission of light (FDSS 6000 Hamamatsu) for a period of 90 s. Antagonist activity was tested on the same preparation: in the case of sst receptors, following the addition and 15 min incubation with 100 μ L of the reference agonist (SST28, Bachem, H4955), and in the case of MCH₁, following the addition and 3 min incubation with 30 μ L of the reference agonist (MCH, Bachem, H1482). In both cases, the reference agonist was used at a final concentration equivalent to the EC₈₀ determined for the same experimental day (using the reader injection system). All values were normalized relative to background (defined as 0%) and the maximal response to SST28 or MCH (defined as 100%), respectively. EC₅₀ values were calculated by nonlinear regression analysis using a sigmoidal dose–response model (XLfit, IDBS Software).

Molecular Modeling Studies. All pyranose compounds were created initially as 2D SLN strings using the Sybyl package from Tripos. The three-dimensional structures of the compounds were generated using an industry-standard 3D structure generator (Concord) and further energy minimized, using the MMFF94s force field, creating a single, low energy conformation for each compound. The four descriptors were calculated using Sybyl (Tripos) using in-house SPL scripting.

Selected compounds have undergone a systematic conformational analysis procedure, which included a systematic variation of the ring conformation of the pyranose ring, followed by a systematic variation of the first rotatable torsional angle of each substituent. All feasible conformations were then energy minimized, discarding all conformations with energy greater than 5 kcal from the lowest energy conformation. In addition, from this set of low energy conformations only conformations were selected which had an rmsd of heavy atom position greater than 1 Å from any other conformation. This procedure, which was implemented within Sybyl using the built-in Systematic Search method extended with in-house scripting, generated a set of low energy and diverse conformers for the selected compounds.

Library Production Process. Practically, all glycosides **2** (benzyl 2-azido-3-*O*-benzoyl-6-*O*-(*tert*-butyldiphenylsilyl)-2-deoxy- α/β -D-glucopyranoside **2a**, (naphth-2-yl)methyl 2-azido-3-*O*-benzoyl-6-*O*-(*tert*-butyldiphenylsilyl)-2-deoxy- α/β -D-glucopyranoside **2b**, 2'-(phenyl)ethyl 2-azido-3-*O*-benzoyl-6-*O*-(*tert*-butyldiphenylsilyl)-2-deoxy- α/β -D-glucopyranoside **2c**, 4'-chlorobenzyl 2-azido-3-*O*-benzoyl-6-*O*-(*tert*-butyldiphenylsilyl)-2-deoxy- α/β -D-glucopyranoside **2d**, benzyl 2-azido-3-*O*-benzoyl-6-*O*-(*tert*-butyldiphenylsilyl)-

2-deoxy- α/β -D-allopyranoside **2e**, (naphth-2-yl)methyl 2-azido-3-*O*-benzoyl-6-*O*-(*tert*-butyldiphenylsilyl)-2-deoxy- α/β -D-allopyranoside **2f**, 2'-(phenyl)ethyl 2-azido-3-*O*-benzoyl-6-*O*-(*tert*-butyldiphenylsilyl)-2-deoxy- α/β -D-allopyranoside **2g**, 4'-chlorobenzyl 2-azido-3-*O*-benzoyl-6-*O*-(*tert*-butyldiphenylsilyl)-2-deoxy- α/β -D-allopyranoside **2h**) were prepared in solution as α/β mixtures (details are provided in the Supporting Information). All glycoside products as well as the Glc-SMe and All-SMe building blocks²³ were then attached to the resin. Resin loading determination was performed by subjecting a known amount of resin to cleavage and diluting the filtrate to a known volume. The concentration of the sugar was assessed by HPLC/UV comparison to a standard curve, and the resulting resin loading value was derived.

The library synthesis was performed following the “split-and-pool” technique, using the IRORI directed sorting process and the Synthesis Manager software. Each individual resin was split in the desired number of Kan microreactors. Around 80 mg of resin was introduced in each Kan, using the IRORI dry resin filler. Each microreactor contained a unique tag identifier (ceramic 2D-coded cap). By pooling microreactors into common building block groups, the directed sorting process made the synthesis efficient while enabling the synthesis of one discrete compound in each microreactor. Quality control (QC) Kans were added to monitor evolution of each reaction along the library production process.

When the synthetic process was completed, the Kans were transferred into BOHDAN blocks for cleavage off-resin. The discrete crude compounds were collected and purified by preparative LC/MS. The purified samples were reanalyzed by LC/MS with parallel ELSD detection and weighted after drying to determine yield and purity. A sample synthesis was judged successful if it demonstrated the correct MH⁺ value in MS and was obtained with a yield greater than 1 mg and a purity by ELSD greater than 85%. The list of the 287 successful samples obtained in this way, along with the yield and C-18 HPLC retention time, is provided as Supporting Information.

Resynthesis of Actives As Individual Anomers. Individual anomer products were obtained using the same solid phase synthetic route as described,²² but starting from a single anomer glycoside, obtained after column chromatography of the α/β glycosides.

Compounds **8 h- α** , **8 h- β** , and **8a** were synthesized and characterized in detail elsewhere.²²

(Naphth-2-yl)methyl 2-(4'-Aminobutyrylamido)-3-*O*-(4'-chlorobenzyl)-2-deoxy-6-*O*-methyl- α -D-glucopyranoside (8d- α). Resin loaded glycoside **2b- α** (80 mg resin, 0.35 mmol/g) was carried through the solid phase synthetic process. The title product was isolated by HPLC purification and MS detection as a white solid (6.7 mg, 44%). ¹H NMR (500 MHz, DMSO-*d*₆) δ 1.73 (m, 2 H, NHCOCH₂CH₂CH₂NH₂), 2.23 (t, 2H, *J* = 7.2 Hz, NHCOCH₂CH₂CH₂NH₂), 2.79 (t, 2H, *J* = 7.5 Hz, NHCOCH₂CH₂CH₂NH₂), 3.30 (s, 3H, OCH₃), 3.35–3.42 (m, 1H, H-4), 3.53 (dd, 1H, *J*_{H5,H6a} = 5.8 Hz, *J*_{H6a,H6b} = 10.7 Hz, H-6a), 3.61 (dd, 1H, *J*_{H5,H6b} = 0.5 Hz, H-6b), 3.63–3.69 (m, 1H, H-3), 3.70–3.76 (ddd, 1H, H-5), 3.88–3.95 (m, 1H, H-2), 4.63, (d, 1H, *J*_{A,B} = 11.6 Hz, OCH₂(B)-Ar¹), 4.64 (d, 1H, *J*_{A,B} = 12.7 Hz, OCH₂(B)-Ar²), 4.82 (d, 1H, OCH₂(A)-Ar¹), 4.76 (d, 1H, *J*_{H1,H2} = 3.5 Hz, H-1), 4.85 (d, 1H, OCH₂(A)-Ar²), 5.47 (d, 1H, *J*_{OH,H-4} = 7.0 Hz, OH-4), 7.31–7.40 (m, 4H, aromat H), 7.50–7.58 (m, 3H,

aromat H), 7.61–7.78 (bs, 3H, NH₃), 7.88–7.97 (m, 4H, aromat H), 8.17 (d, 1H, $J_{\text{NH,H-2}} = 8.8$ Hz, C-2NH). ¹³C NMR (125.7 MHz, DMSO-*d*₆) δ 22.95 (CH₂CH₂CH₂), 31.72 (COCH₂), 40.34 (H₂NCH₂), 52.17 (C-2), 58.4 (OCH₃), 68.25 (OCH₂Ar²), 70.26 (C-4), 71.36 (C-6), 71.62 (C-5), 72.46 (OCH₂Ar¹), 79.63 (C-3), 96.1 (C-1), 125.79, 125.88, 126.14, 126.22, 127.46, 127.51, 127.76, 128.84, 128.94, 131.51, 132.37, 132.61, (all aromat C), 171.28 (NHCO). HRMS (ESI, pos mode) *m/z* [M + H]⁺ calcd for C₂₉H₃₆C₁₁N₂O₆ 543.2256; found 543.2254.

(Naphth-2-yl)methyl 2-(4'-Aminobutyrylamido)-3-O-(4'-chlorobenzyl)-2-deoxy-6-O-methyl-β-D-glucopyranoside (8d-β). Resin loaded glycoside **2b-β** (80 mg resin, 0.37 mmol/g) was carried through the solid phase synthetic process. The title product was isolated by HPLC purification and MS detection as a white solid (4.6 mg, 29%). ¹H NMR (600 MHz, DMSO-*d*₆) δ 1.63–1.69 (m, 2H, NHCOCH₂CH₂CH₂NH₂(A,B), 2.03–2.22 (m, 2H, NHCOCH₂CH₂CH₂NH₂), 2.76 (m, 1H, $J = 7.6$ Hz, NHCCH₂-CH₂CH₂NH₂ (A)), 3.10–3.17 (m, 1H, $J = 7.6$ Hz, NHCCH₂-CH₂CH₂NH₂ (B)), 3.25 (s, 3H, OCH₃), 3.27–3.59 (m, 4H, H-3, H-4, H-5, H-6a), 3.67 (dd, 1H, $J_{\text{H5,H6b}} = 0.5$ Hz, $J_{\text{H6a,H6b}} = 10.6$ Hz, H-6b), 3.70–3.83 (m, 1H, H-2), 4.48 (d, 1H, $J_{\text{H1,H2}} = 8.1$ Hz, H-1), 4.55 (d, 1H, $J_{\text{A,B}} = 11.7$ Hz, OCH₂(B)Ar¹), 4.59 (d, 1H, OCH₂(B)Ar¹), 4.70 (d, 1H, $J_{\text{A,B}} = 12.7$ Hz, OCH₂(B)Ar²), 4.76 (d, 1H, $J_{\text{A,B}} = 11.7$ Hz, OCH₂(A)Ar¹), 4.91 (d, 1H, OCH₂(A)Ar²), 5.32 (d, 1H, $J_{\text{OH,H-4}} = 6.7$ Hz, OH-4(B)), 5.40–5.45 (m, 1H, OH-4(A)), 6.52 (bs, 1H, NH₂), 6.66 (m, 1H, NH₂), 7.27–7.55 (m, 7H, aromat H), 7.79–7.95 (m, 4H, aromat H), 8.01 (d, 1H, $J_{\text{NH,H-2}} = 9.1$ Hz, C-2NH), 9.40 (bs, 1H, NH₃). HMBC (599.72 MHz/150.815 MHz, DMSO-*d*₆) δ 23.73 (CH₂CH₂CH₂)(A), 24.43 (CH₂CH₂CH₂)(B), 32.28 (COCH₂), 38.73 (H₂NCH₂), 52.32 (C-2), 58.42 (OCH₃), 69.43 (OCH₂-Naph), 69.90 (C-4(B)), 70.49 (C-4(A)), 71.32 (C-6), 72.13 (OCH₂Ar), 75.41 (C-5), 79.51 (C-3(B)), 82.21 (C-3(A)), 100.14 (H-1), 125.57, 125.69, 125.92, 127.56, 127.80, 128.85, 131.43, 131.55, 132.13, 132.37, 132.60, 135.30, 137.99 (all aromat C), 170.93 (NHCO)(A), 171.16 (NHCO)(B). HRMS (ESI, pos mode) *m/z* [M + H]⁺ calcd for C₂₉H₃₆C₁₁N₂O₆ 543.2256; found 543.2259.

(Naphth-2-yl)methyl 2-(3'-Aminopropionylamido)-2-deoxy-6-O-methyl-3-O-(naphth-2-yl)methyl-β-D-allopyranoside (8e-β). Resin loaded glycoside **2f-β** (80 mg resin, 0.3 mmol/g) was carried through the solid phase synthetic process. The title product was isolated by HPLC purification and MS detection as a white solid (2.1 mg, 16%). ¹H NMR (500 MHz, DMSO-*d*₆) δ 2.43–2.56 (m, 2H, NHCOCH₂CH₂NH₂), 2.88 (t, 2H, $J = 6.8$ Hz, NHCOCH₂-CH₂NH₂), 3.02–3.10 (dq, 2H, NHCOCH₂CH₂CH₂NH₂), 3.31 (s, 3H, OCH₃), 3.54 (dd, 1H, $J_{\text{H5,H6}} = 5.9$ Hz, $J_{\text{H6a,H6b}} = 10.8$ Hz, H-6a), 3.57–3.64 (m, 1H, H-4), 3.68 (d, 1H, $J_{\text{H5,H6b}} = 0.5$ Hz, H-6b), 3.82 (m, 1H, H-2), 3.88–3.96 (m, 2H, H-3, H-5), 4.71 (d, 1H, $J_{\text{A,B}} = 12.1$ Hz, OCH₂(B)-Ar¹), 4.83 (d, 1H, $J_{\text{A,B}} = 11.9$ Hz, OCH₂(B)-Ar²), 4.83 (d, 1H, $J_{\text{H1,H2}} = 7.8$ Hz, H-1), 4.92 (d, 1H, OCH₂(A)-Ar¹), 4.99 (d, 1H, OCH₂(A)-Ar²), 5.32 (d, 1H, $J_{\text{OH,H-4}} = 5.5$ Hz, OH-4), 7.46–7.55 (m, 5H, aromat H), 7.62 (d, 1H, aromat H), 7.66–7.78 (bs, 2H, NH₂), 7.81–7.93 (m, 8H, aromat H), 8.28 (d, 1H, $J_{\text{NH,H-2}} = 8.1$ Hz, C-2NH). ¹³C NMR (125.7 MHz, DMSO-*d*₆) δ 31.78 (COCH₂), 35.16 (H₂NCH₂), 52.65 (C-2), 58.53 (OCH₃), 67.98 (OCH₂Ar²), 70.02 (C-4), 71.89, 73.64, 74.41, 77.81, (3 sugar carbons, and OCH₂Ar¹), 98.42 (C-1), 125.67, 125.76, 125.80, 125.81, 125.94, 126.02, 126.18, 127.38, 127.40, 127.55, 127.59, 132.28, 132.60, 135.45, 136.42, (all aromat C), 156.61, 157.86 (TFA + TFA-salt), 169.00 (NHCO). HRMS (ESI, pos mode) *m/z* [M + H]⁺ calcd for C₃₂H₃₇N₂O₆ 545.2646; found 545.2639.

(4'-Chlorobenzyl) 3-O-(4'-Chlorobenzyl)-2-deoxy-2-(4'-guanidinobutyrylamido)-6-O-methyl-α-D-glucopyranoside (9c-α). Resin loaded glycoside **2d-α** (80 mg resin, 0.26 mmol/g) was carried through the solid phase synthetic process. The title product was isolated by HPLC purification and MS detection as a white solid (5.8 mg, 49%). ¹H NMR (500 MHz, DMSO-*d*₆) δ 1.60–1.70 (m, 2H, NHCOCH₂CH₂CH₂NH), 2.16 (t, 2H, $J = 7.3$ Hz, NHCOCH₂CH₂CH₂NH), 3.07 (q, 2H, NHCOCH₂CH₂CH₂NH), 3.28

(s, 3H, OCH₃), 3.36 (dd 1H, H-4), 3.50 (dd, 1H, $J_{\text{H5,H6a}} = 5.7$ Hz, $J_{\text{H6a,H6b}} = 10.7$ Hz, H-6a), 3.58 (dd, 1H, $J_{\text{H5,H6a}} = 0.5$ Hz, H-6b), 3.60–3.66 (m, 2H, H-3, H-5), 3.89 (ddd, 1H, H-2), 4.46 (d, 1H, $J_{\text{A,B}} = 12.6$ Hz, OCH₂(B)-Ar²), 4.62 (d, 1H, $J_{\text{A,B}} = 11.6$ Hz, OCH₂(B)-Ar¹), 4.65 (d, 1H, OCH₂(A)-Ar¹), 4.70 (d, 1H, $J_{\text{H1,H2}} = 3.4$ Hz, H-1), 4.81 (d, 1H, OCH₂(A)-Ar²), 5.45 (d, 1H, $J_{\text{OH,H-4}} = 6.9$ Hz, OH-4), 7.29–7.46 (m, 8H, aromat. H), 7.59 (m, 1H, NH), 8.12 (d, 1H, $J_{\text{NH,H-2}} = 8.7$ Hz, C-2NH). ¹³C NMR (125.7 MHz, DMSO-*d*₆) δ 24.55 (CH₂CH₂CH₂), 31.68 (COCH₂), 40.34 (H₂NCH₂), 52.13 (C-2), 58.37 (OCH₃), 67.28 (OCH₂Ar²), 70.22 (C-4), 71.32 (C-6), 71.60 (C-5), 72.50 (OCH₂Ar¹), 79.60 (C-3), 96.22 (C-1), 127.80, 128.08, 128.90, 129.34, 131.49, 132.04, 136.58, 138.22 (all aromat C), 156.65 (guanidine C), 171.73 (NHCO). HRMS (ESI, pos mode) *m/z* [M + H]⁺ calcd for C₂₆H₃₅-Cl₂N₄O₆ 569.1928; found 569.1917.

(4'-Chlorobenzyl) 3-O-(4'-Chlorobenzyl)-2-deoxy-2-(4'-guanidinobutyrylamido)-6-O-methyl-β-D-glucopyranoside (9c-β). Resin loaded glycoside **2d-β** (80 mg resin, 0.34 mmol/g) was carried through the solid phase synthetic process. The title product was isolated by HPLC purification and MS detection as a white solid (8.8 mg, 57%). ¹H NMR (600 MHz, DMSO-*d*₆) δ 1.61–1.69 (m, 2H, NHCOCH₂CH₂CH₂NH), 2.06–2.14 (m, 2H, NHCOCH₂-CH₂CH₂NH), 3.06 (q, 2H, NHCOCH₂CH₂CH₂NH), 3.30 (s, 3H, OCH₃), 3.20–3.30 (m, 2H, H-4, H-5), 3.43 (dd, 1H, H-3), 3.49 (dd, 1H, $J_{\text{H5,H6}} = 4.2$ Hz, $J_{\text{H6a,H6b}} = -10.7$ Hz, H-6a), 3.64 (d, 1H, $J_{\text{H5,H6b}} = 0.5$ Hz, H-6b), 3.69 (m, 1H, H-2), 4.42 (d, 1H, $J_{\text{H1,H2}} = 8.4$ Hz, H-1), 4.51 (d, 1H, $J_{\text{A,B}} = 12.7$ Hz, OCH₂(B)-Ar¹), 4.54 (d, 1H, $J_{\text{A,B}} = 11.8$ Hz, OCH₂(B)-Ar²), 4.73 (d, 1H, OCH₂(A)-Ar¹), 4.77 (d, 1H, OCH₂(A)-Ar²), 5.44 (d, 1H, $J_{\text{OH,H-4}} = 4.3$ Hz, OH-4), 7.28–7.46 (m, 8H, aromat H), 7.67 (bs, 1H, NH), 8.03 (d, 1H, $J_{\text{NH,H-2}} = 9.1$ Hz, C-2NH). HMBC (600 MHz/150.8 MHz, DMSO-*d*₆) δ 24.55 (CH₂CH₂CH₂), 32.05 (COCH₂), 40.02 (H₂NCH₂), 53.73 (C-2), 58.42 (OCH₃), 68.61 (OCH₂Ar¹), 69.78 (C-4), 71.31 (C-6), 72.13 (OCH₂Ar²), 75.41 (C-5), 82.21 (C-3), 100.14 (C-1), 127.68, 128.03, 128.85, 131.43, 131.67, 131.78, 136.94, 137.88 (all aromat C), 156.63 (guanidino carbon), 171.40 (NHCO). HRMS (ESI, pos mode) *m/z* [M + H]⁺ calcd for C₂₆H₃₅Cl₂N₄O₆ 569.1928; found 569.1935.

(Naphth-2-yl)methyl 3-O-(4'-Chlorobenzyl)-2-deoxy-2-(4'-guanidinobutyrylamido)-6-O-methyl-α-D-glucopyranoside (9d-α). Resin loaded glycoside **2b-α** (80 mg resin, 0.35 mmol/g) was carried through the solid phase synthetic process. The title product was isolated by HPLC purification and MS detection as a white solid (10.5 mg, 64%). ¹H NMR (500 MHz, DMSO-*d*₆) δ 1.59–1.68 (m, 2H, NHCOCH₂CH₂CH₂NH), 2.18 (t, 2H, $J = 7.3$ Hz, NHCOCH₂CH₂CH₂NH), 3.06 (q, 2H, NHCOCH₂CH₂CH₂NH), 3.30 (s, 3H, OCH₃), 3.38 (dd 1H, H-4), 3.52 (dd, 1H, $J_{\text{H5,H6a}} = 5.7$ Hz, $J_{\text{H6a,H6b}} = 10.7$ Hz, H-6a), 3.61 (dd, 1H, $J_{\text{H5,H6a}} = 0.5$ Hz, H-6b), 3.65 (dd, 1H, $J_{\text{H3,H4}} = 8.8$ Hz, $J_{\text{H2,H3}} = 10.7$ Hz, H-3), 3.72 (m, 1H, H-5), 3.91 (ddd, 1H, H-2), 4.63 (dd, 2H, OCH₂(B)-Ar¹, OCH₂(B)-Ar²), 4.76 (d, 1H, $J_{\text{H1,H2}} = 3.4$ Hz, H-1), 4.83 (t, 2H, OCH₂(A)-Ar¹, OCH₂(A)-Ar²), 5.46 (d, 1H, $J_{\text{OH,H-4}} = 7.0$ Hz, OH-4), 7.30–7.38 (m, 4H, aromat H), 7.49–7.57 (m, 3H, aromat H), 7.57–7.64 (m, 1H, NH), 7.86–7.95 (m, 4H, aromat H), 8.16 (d, 1H, $J_{\text{NH,H-2}} = 8.7$ Hz, C-2NH). ¹³C NMR (125.7 MHz, DMSO-*d*₆) δ 24.56 (CH₂CH₂CH₂), 31.70 (COCH₂), 40.34 (H₂NCH₂), 52.18 (C-2), 58.39 (OCH₃), 68.22 (OCH₂Ar²), 70.26 (C-4), 71.38 (C-6), 71.63 (C-5), 72.46 (OCH₂Ar¹), 79.64 (C-3), 96.11 (C-1), 125.83, 125.87, 126.13, 126.23, 127.44, 127.49, 127.73, 127.80, 128.92, 131.49, 132.36, 132.60, 135.05, 138.22 (all aromat C), 156.66 (guanidine C), 171.71 (NHCO). HRMS (ESI, pos mode) *m/z* [M + H]⁺ calcd for C₃₀H₃₈Cl₁N₄O₆ 585.2474; found 585.2466.

(Naphth-2-yl)methyl 3-O-(4'-Chlorobenzyl)-2-deoxy-2-(4'-guanidinobutyrylamido)-6-O-methyl-β-D-glucopyranoside (9d-β). Resin loaded glycoside **2b-β** (80 mg resin, 0.37 mmol/g) was carried through the solid phase synthetic process. The title product was isolated by HPLC purification and MS detection as a white solid (5.9 mg, 34%). ¹H NMR (600 MHz, DMSO-*d*₆) δ 1.61–1.72 (m, 2H, NHCOCH₂CH₂CH₂NH), 2.06–2.16 (m, 2H, NHCOCH₂-CH₂CH₂NH), 3.07 (q, 2H, NHCOCH₂CH₂CH₂NH), 3.32 (s, 3H,

OCH₃), 3.30–3.37 (m, 2H, H-4, H-5), 3.44 (dd, 1H, H-3), 3.51 (dd, 1H, $J_{H5,H6} = 4.5$ Hz, $J_{H6a,H6b} = 10.7$ Hz, H-6a), 3.67 (d, 1H, $J_{H5,H6b} = 0.5$ Hz, H-6b), 3.74 (m, 1H, H-2), 4.49 (d, 1H, $J_{H1,H2} = 8.1$ Hz, H-1), 4.51 (d, 1H, $J_{A,B} = 11.8$ Hz, OCH₂(B)-Ar¹), 4.69 (d, 1H, $J_{A,B} = 12.7$ Hz, OCH₂(B)-Ar²), 4.77 (d, 1H, OCH₂(A)-Ar¹), 4.91 (d, 1H, OCH₂(A)-Ar²), 5.43 (d, 1H, $J_{OH,H-4} = 5.5$ Hz, OH-4), 7.27–7.44 (m, 5H, aromat H), 7.48–7.57 (m, 3H, aromat. H, NH-CH₂), 7.77–7.94 (m, 4H, aromat H), 8.03 (d, 1H, $J_{NH,H-2} = 9.2$ Hz, C-2NH). HMBC (600 MHz/150.8 MHz, DMSO-*d*₆) δ 24.55 (CH₂CH₂CH₂), 32.05 (COCH₂), 40.02 (H₂NCH₂), 53.73 (C-2), 58.42 (OCH₃), 69.43 (OCH₂Ar¹), 69.78 (C-4), 71.31 (C-6), 72.13 (OCH₂Ar²), 75.29 (C-5), 82.21 (C-3), 100.02 (C-1), 125.45, 125.57, 125.69, 125.92, 127.33, 127.56, 127.68, 128.85, 131.43, 132.13, 132.60, 135.30, 137.99 (all aromat C), 156.51 (guanidino carbon), 171.40 (NH-CO). HRMS (ESI, pos mode) m/z [M + H]⁺ calcd for C₃₀H₃₈Cl₁N₄O₆ 585.2474; found 585.2469.

4'-Chlorobenzyl 2-Deoxy-2-(4'-guanidinobutyrylamido)-6-O-methyl-3-O-(naphth-2-yl)methyl- α -D-glucopyranoside (9e- α). Resin loaded glycoside **2d- α** (80 mg resin, 0.26 mmol/g) was carried through the solid phase synthetic process. The title product was isolated by HPLC purification and MS detection as a white solid (7.9 mg, 65%). ¹H NMR (600 MHz, DMSO-*d*₆) δ 1.60–1.71 (m, 2 H, NHCOCH₂CH₂CH₂NH), 2.15–2.24 (m, 2H, NHCOCH₂CH₂CH₂NH), 3.06 (q, 2H, NHCOCH₂CH₂CH₂NH), 3.29 (s, 3H, OCH₃), 3.41 (dd 1 H, H-4), 3.52 (dd, 1H, $J_{H5,H6a} = 5.8$ Hz, $J_{H6a,H6b} = 10.7$ Hz, H-6a), 3.60 (dd, 1H, $J_{H5,H6a} = 0.5$ Hz, H-6b), 3.64–3.72 (m, 2H, H-3, H-5), 3.94 (ddd, 1 H, H-2), 4.47 (d, 1H, $J_{gem} = 12.6$ Hz, OCH₂(B)-Ar¹), 4.67 (d, 1H, OCH₂(A)-Ar¹), 4.72 (d, 1H, $J_{H1,H2} = 3.5$ Hz, H-1), 4.81 (d, 1H, $J_{gem} = 11.6$ Hz, OCH₂(B)-Ar²), 4.99 (d, 1H, OCH₂(A)-Ar²), 5.50 (d, 1H, $J_{OH,H-4} = 6.7$ Hz, OH-4), 7.39–7.53 (m, 7H, aromat H), 7.56–7.64 (m, 1 H, NH), 7.76–7.92 (m, 4H, aromat H), 8.20 (d, 1 H, $J_{NH,H-2} = 8.5$ Hz, C-2NH). HMBC (600 MHz/150.8 MHz, DMSO-*d*₆) δ 24.55 (CH₂CH₂CH₂), 31.58 (COCH₂), 40.13 (H₂NCH₂), 52.09 (C-2), 58.30 (OCH₃), 67.21 (OCH₂Ar¹), 70.24 (C-4), 71.31 (C-6), 71.43 (C-5), 73.42 (OCH₂Ar²), 79.51 (C-3), 96.15 (C-1), 124.63, 125.22, 125.57, 125.81, 127.33, 127.56, 129.20, 132.02, 132.13, 132.60, 132.72, 136.59, 136.82 (all aromat C), 156.516 (guanidine C), 171.75 (NH-CO). HRMS (ESI, pos mode) m/z [M + H]⁺ calcd for C₃₀H₃₈Cl₁N₄O₆ 585.2474; found 585.2466.

4'-Chlorobenzyl 2-Deoxy-2-(4'-guanidinobutyrylamido)-6-O-methyl-3-O-(naphth-2-yl)methyl- β -D-glucopyranoside (9e- β). Resin loaded glycoside **2d- β** (80 mg resin, 0.34 mmol/g) was carried through the solid phase synthetic process. The title product was isolated by HPLC purification and MS detection as a white solid (7.8 mg, 49%). ¹H NMR (600 MHz, DMSO-*d*₆) δ 1.61–1.69 (m, 2H, NHCOCH₂CH₂CH₂NH), 2.10 (t, 2H, $J_{A,B} = 7.1$ Hz NHCOCH₂CH₂CH₂NH), 3.04 (q, 2H, NHCOCH₂CH₂CH₂NH), 3.32 (s, 3H, OCH₃), 3.29–3.36 (m, 2H, H-4, H-5), 3.47–3.55 (m, 2H, H-3, H-6a), 3.66 (d, 1H, $J_{H6a,H6b} = 10.7$ Hz, $J_{H5,H6b} = 0.5$ Hz, H-6b), 3.74 (m, 1H, H-2), 4.45 (d, 1H, $J_{H1,H2} = 8.1$ Hz, H-1), 4.52 (d, 1H, $J_{A,B} = 12.7$ Hz, OCH₂(B)-Ar¹), 4.72–4.77 (m, 2H, OCH₂(A)-Ar¹, OCH₂(B)-Ar²), 4.95 (d, 1H, $J_{A,B} = 11.7$ Hz, OCH₂(A)-Ar²), 5.48 (d, 1H, $J_{OH,H-4} = 5.1$ Hz, OH-4), 7.31 (d, 2 H, $J = 8.4$ Hz, aromat H), 7.39 (d, 2 H, $J = 8.4$ Hz, aromat H), 7.43–7.52 (m, 3H, aromat H), 7.67 (bs, 1H, NH-CH₂), 7.78 (s, 1H, aromat H), 7.83–7.92 (m, 3H, aromat H), 8.06 (d, 1H, $J_{NH,H-2} = 9.1$ Hz, C-2NH). HMBC (600 MHz/150.8 MHz, DMSO-*d*₆) δ 24.55 (CH₂CH₂CH₂), 32.05 (COCH₂), 40.02 (H₂NCH₂), 53.73 (C-2), 58.42 (OCH₃), 68.61 (OCH₂Ar¹), 69.90 (C-4), 71.31 (C-6), 73.18 (OCH₂Ar²), 75.41 (C-5), 82.21 (C-3), 100.26 (C-1), 125.34, 125.45, 125.69, 125.81, 127.45, 127.92, 128.85, 131.78, 132.13, 132.49, 132.60, 136.47, 136.71, 136.82 (all aromat C), 156.51 (guanidino carbon), 171.40 (NH-CO). HRMS (ESI, pos mode) m/z [M + H]⁺ calcd for C₃₀H₃₈Cl₁N₄O₆ 585.2474; found 585.2471.

2-(Phenyl)ethyl 3-O-(4'-Chlorobenzyl)-2-deoxy-2-(4'-guanidinobutyrylamido)-6-O-methyl- α -D-glucopyranoside (9f- α). Resin loaded glycoside **2c- α** (80 mg resin, 0.45 mmol/g) was carried through the solid phase synthetic process. The title product was isolated by HPLC purification and MS detection as a white solid

(15.7 mg, 749%). ¹H NMR (500 MHz, DMSO-*d*₆) δ 1.61–1.69 (m, 2 H, NHCOCH₂CH₂CH₂NH), 2.15 (t, 2H, $J = 7.3$ Hz, NHCOCH₂CH₂CH₂NH), 2.86 (t, 2H, $J = 6.9$ Hz, NHCOCH₂CH₂CH₂NH), 3.08 (q, 2 H, CH₂-Ar¹), 3.24 (s, 3H, OCH₃), 3.32 (m, 1 H, H-4), 3.44 (dd, 1H, $J_{H5,H6a} = 5.8$ Hz, $J_{H6a,H6b} = 10.7$ Hz, H-6a), 3.47–3.57 (m, 3H, H-3, H-5, H-6b), 3.58–3.64 (m, 1H, OCH₂CH₂(A)), 3.73–3.80 (m, 1H, OCH₂CH₂(B)), 3.85 (ddd, 1 H, H-2), 4.61 (d, 1H, $J_{A,B} = 11.6$ Hz, OCH₂(B)-Ar²), 4.68 (d, 1H, $J_{H1,H2} = 3.5$ Hz, H-1), 4.79 (d, 1H, OCH₂(A)-Ar²), 5.41 (d, 1H, $J_{OH,H-4} = 6.6$ Hz, OH-4), 7.18–7.23 (t, 1 H, aromat H), 7.24–7.39 (m, 8H, aromat H), 7.62 (m, 1 H, NH), 7.90 (d, 1 H, $J_{NH,H-2} = 8.8$ Hz, C-2NH). ¹³C NMR (125.7 MHz, DMSO-*d*₆) δ 24.54 (CH₂CH₂CH₂), 31.72 (COCH₂), 35.02 (CH₂Ar), 40.34 (H₂NCH₂), 52.13 (C-2), 58.30 (OCH₃), 67.71 (OCH₂Ar²), 70.18 (C-4), 71.27, 71.38, (C-5* C-6*), 72.41 (OCH₂Ar¹), 79.63 (C-3), 96.59 (C-1), 125.98, 127.79, 128.09, 128.70, 128.96, 131.49, 138.24, 138.65, (all aromat C), 156.69 (guanidine C), 171.66 (NH-CO). HRMS (ESI, pos mode) m/z [M + H]⁺ calcd for C₂₇H₃₈Cl₁N₄O₆ 549.2474; found 549.2473.

(Naphth-2-yl)methyl 2-Deoxy-2-(4'-guanidinobutyrylamido)-6-O-methyl-3-O-(naphth-2-yl)methyl- α -D-glucopyranoside (9g- α). Resin loaded glycoside **2b- α** (80 mg resin, 0.35 mmol/g) was carried through the solid phase synthetic process. The title product was isolated by HPLC purification and MS detection as a white solid (9.7 mg, 58%). ¹H NMR (500 MHz, DMSO-*d*₆) δ 1.59–1.70 (m, 2 H, NHCOCH₂CH₂CH₂NH), 2.17–2.26 (m, 2H, NHCOCH₂CH₂CH₂NH), 3.05 (q, 2H, NHCOCH₂CH₂CH₂NH), 3.32 (s, 3H, OCH₃), 3.43 (dd 1 H, H-4), 3.54 (dd, 1H, $J_{H5,H6a} = 5.7$ Hz, $J_{H6a,H6b} = 10.7$ Hz, H-6a), 3.63 (dd, 1H, $J_{H5,H6a} = 0.5$ Hz, H-6b), 3.69–3.79 (m, 2H, H-3, H-5), 3.96 (ddd, 1 H, H-2), 4.65 (dd, 1H, $J_{gem} = 12.4$ Hz, OCH₂(B)-Ar¹), 4.78 (d, 1H, $J_{H1,H2} = 3.4$ Hz, H-1), 4.82 (d, 1H, $J_{gem} = 11.6$ Hz, OCH₂(B)-Ar²), 4.86 (d, 1H, OCH₂(A)-Ar¹), 5.00 (d, 1H, OCH₂(A)-Ar²), 5.50 (d, 1H, $J_{OH,H-4} = 7.0$ Hz, OH-4), 7.44–7.64 (m, 7H, 6 aromat H, NH), 7.77–7.96 (m, 8H, aromat H), 8.22 (d, 1 H, $J_{NH,H-2} = 8.7$ Hz, C-2NH). ¹³C NMR (125.7 MHz, DMSO-*d*₆) δ 24.58 (CH₂CH₂CH₂), 31.74 (COCH₂), 40.34 (H₂NCH₂), 52.27 (C-2), 58.41 (OCH₃), 68.22 (OCH₂Ar²), 70.35 (C-4), 71.43 (C-6), 71.68 (C-5), 72.45 (OCH₂Ar¹), 79.66 (C-3), 96.16 (C-1), 125.34, 125.80, 125.84, 125.865, 125.869, 125.91, 126.13, 126.229, 126.233, 127.32, 127.38, 127.44, 127.45, 127.50, 127.74, 132.21, 132.37, 132.61, 135.08, 136.86 (all aromat C), 156.66 (guanidine C), 171.75 (NH-CO). HRMS (ESI, pos mode) m/z [M + H]⁺ calcd for C₃₄H₄₁N₄O₆ 601.3021; found 601.3019.

Acknowledgment. The research described herein was in part supported by a Smart Futures Fund from the Queensland Government through a National and International Research Alliances Program entitled: Application of Alchemia's Drug Discovery Platform (VAST) to discover new drug candidates for selected G-Protein coupled receptors (GPCRs).

Supporting Information Available: Experimental details for the FKW tripeptide distance analysis, synthetic details of the library synthesis, and NMR spectral data (¹H, ¹³C or HMBC, and COSY) for compounds **8d- α** , **8d- β** , **8e- β** , **9c- α** , **9c- β** , **9d- α** , **9d- β** , **9e- α** , **9e- β** , **9f- α** , and **9g- α** . This material is available free of charge via the Internet at <http://pubs.acs.org>.

References

- (1) Jones, R. M.; Boatman, P. D.; Semple, G.; Shin, Y. J.; Tamura, S. Y. Clinically validated peptides as templates for de novo peptidomimetic drug design at G-protein-coupled receptors. *Curr. Opin. Pharmacol.* **2003**, *3*, 530–543.
- (2) Hirschmann, R.; Nicalou, K. C.; Pietranico, S.; Salvino, J.; Leahy, E. M.; Sprngeler, P. A.; Furst, G.; Amos B. Smith, I. Nonpeptidic Peptidomimetics with a β -D-Glucose Scaffolding. A Partial Somatostatin Agonist Bearing a Close Structural Relationship to a Potent, Selective Substance P Antagonist. *J. Am. Chem. Soc.* **1992**, *114*, 9217–9218.
- (3) Hirschmann, R.; Yao, W.; Cascieri, M. A.; Strader, C. D.; Maechler, L.; Cichy-Knight, M. A.; John Hynes, J.; van Rijn, R. D.; Sprengler, P. A.; Amos B. Smith, I. Synthesis of Potent Cyclic Hexapeptide

- NK-1 Antagonists. Use of a Minilibrary in Transforming a Peptidic Somatostatin Receptor Ligand into an NK-1 Receptor Ligand via a Polyvalent Peptidomimetic. *J. Med. Chem.* **1996**, *39*, 2441–2448.
- (4) Hirschmann, R.; J. H., Jr.; Cichy-Knight, M. A.; van Rijn, R. D.; Sprengeler, P. A.; Spoor, P. G.; Shakespeare, W. C.; Pietranico-Cole, S.; Barbosa, J.; Liu, J.; Yao, W.; Rohrer, S.; Smith, A. B., III Modulation of Receptor and Receptor Subtype Affinities Using Diastereomeric and Enantiomeric Monosaccharide Scaffolds as a Means to Structural and Biological Diversity. A New Route to Ether Synthesis. *J. Med. Chem.* **1998**, *41*, 1382–1391.
- (5) Liu, J.; Underwood, D. J.; Cascieri, M. A.; Rohrer, S. P.; Cantin, L. D.; Chicchi, G.; Smith, A. B., III; Hirschmann, R. Synthesis of a Substance P Antagonist with a Somatostatin Scaffold: Factors Affecting Agonism/Antagonism at GPCRs and the Role of Pseudo-symmetry. *J. Med. Chem.* **2000**, *43*, 3827–3831.
- (6) Hirschmann, R.; Nicolaou, K.; Pietranico, S.; Leahy, E.; Salvino, J. M.; Arison, B.; Cichy, M.; Spoor, P.; Shakespeare, W.; Sprengeler, P.; Hamley, P.; Smith, A., III; Reisine, T.; Raynor, K.; Maechler, L.; Donaldson, C.; Vale, W.; Freidinger, R. M.; Cascieri, M.; Strader, C. D. De Novo Design and Synthesis of Somatostatin Non-Peptide Peptidomimetics Utilizing β -D-Glucose as a Novel Scaffolding. *J. Am. Chem. Soc.* **1993**, *115*, 12550–12568.
- (7) Hirschmann, R.; Sprengeler, P.; Kawasaki, T.; Leahy, J.; Shakespeare, W.; Smith, A., III The versatile steroid nucleus: design and synthesis of a peptidomimetic employing this novel scaffold. *Tetrahedron* **1993**, *49*, 3665–3676.
- (8) Prasad, V.; Birzin, E. T.; McVaugh, C. T.; van Rijn, R. D.; Rohrer, S. P.; Chicchi, G.; Underwood, D. J.; Thornton, E. R.; Smith, A., III; Hirschmann, R. Effects of Heterocyclic Aromatic Substituents on Binding Affinities at Two Distinct Sites of Somatostatin Receptors. Correlation with the Electrostatic Potential of the Substituents. *J. Med. Chem.* **2003**, *46*, 1858–1869.
- (9) Abrous, L.; Hynes, J., Jr.; Friedrich, S. R.; Smith, A. B., III; Hirschmann, R. Design and synthesis of novel scaffolds for drug discovery: hybrids of beta-D-glucose with 1,2,3,4-tetrahydrobenzo-[e][1,4]diazepin-5-one, the corresponding 1-oxazepine, and 2- and 4-pyridyldiazepines. *Org. Lett.* **2001**, *3*, 1089–1092.
- (10) Hirschmann, R.; Ducry, L.; Smith, A. B., III Development of an efficient, regio- and stereoselective route to libraries based on the beta-D-glucose scaffold. *J. Org. Chem.* **2000**, *65*, 8307–8316.
- (11) Angeles, A. R.; Neagu, I.; Birzin, E. T.; Thornton, E. R.; Smith, A. B., III; Hirschmann, R. Synthesis and binding affinities of novel SRIF-mimicking beta-D-glucosides satisfying the requirement for a pi-cloud at C1. *Org. Lett.* **2005**, *7*, 1121–1124.
- (12) Meutermans, W.; Le, G. T.; Becker, B. Carbohydrates as scaffolds in drug discovery. *ChemMedChem* **2006**, *1*, 1164–1194.
- (13) Becker, B.; Condie, G. C.; Le, G. T.; Meutermans, W. Carbohydrate-based scaffolds in drug discovery. *Mini Rev. Med. Chem.* **2006**, *6*, 1299–1309.
- (14) Jensen, K. J.; Brask, J. Carbohydrates as templates for control of distance-geometry in de novo-designed proteins. *Cell. Mol. Life Sci.* **2002**, *59*, 859–869.
- (15) Opatz, T.; Kallus, C.; Wunberg, T.; Schmidt, W.; Henke, S.; Kunz, H. D-Glucose as a multivalent chiral scaffold for combinatorial chemistry. *Carbohydr. Res.* **2002**, *337*, 2089–2110.
- (16) Cervi, G.; Peri, F.; Battistini, C.; Gennari, C.; Nicotra, F. Bicyclic carbohydrate-derived scaffolds for combinatorial libraries. *Bioorg. Med. Chem.* **2006**, *14*, 3349–3367.
- (17) Hunger, U.; Ohnsmann, J.; Kunz, H. Carbohydrate scaffolds for combinatorial syntheses that allow selective deprotection of all four positions independent of the sequence. *Angew. Chem., Int. Ed. Engl.* **2004**, *43*, 1104–1107.
- (18) Gruner, S. A.; Locardi, E.; Lohof, E.; Kessler, H. Carbohydrate-based mimetics in drug design: sugar amino acids and carbohydrate scaffolds. *Chem. Rev.* **2002**, *102*, 491–514.
- (19) Murphy, P. V.; Bradley, H.; Tosin, M.; Pitt, N.; Fitzpatrick, G. M.; Glass, W. K. Development of carbohydrate-based scaffolds for restricted presentation of recognition groups. Extension to divalent ligands and implications for the structure of dimerized receptors. *J. Org. Chem.* **2003**, *68*, 5692–5704.
- (20) Le, G. T.; Abbenante, G.; Becker, B.; Grathwohl, M.; Halliday, J.; Tometzki, G.; Zuegg, J.; Meutermans, W. Molecular diversity through sugar scaffolds. *Drug Discovery Today* **2003**, *8*, 701–709.
- (21) Hobohm, U., S. C. Enlarged representative set of protein structures. *Protein Sci.* **1994**, *3*, 522–524.
- (22) Thanh, G. L.; Adamson, G.; Becker, B.; Clark, C.; Falzun, G. C. T.; Grathwohl, M.; Gupta, P.; Hanson, M.; Huynh, N.; Katavic, P.; Kuipers, K.; Lam, A.; Liu, L.; Mann, M.; Mason, J.; McKeveney, D.; Muldoon, C.; Pearson, A.; Rajaratnam, P.; Ryan, S.; Tometzki, G.; Verquin, G.; Waanders, J.; West, M.; Wilcox, N.; Wimmer, N.; Yau, A.; Zuegg, J.; Meutermans, W. A Versatile Synthetic Approach towards Diversity Libraries using Monosaccharide Scaffolds. *J. Org. Chem.* **2010**, *75*, 197–203.
- (23) Rajaratnam, P. G., P.; Katavic, P.; Kuipers, K.; Huyh, N.; Ryan, S.; Falzun, T.; Tometzki, G.; Bornaghi, L.; Thanh Le, G.; Abbenante, G.; Liu, L.; Meutermans, W. W., N.; West, M. Orthogonally Protected Monosaccharide Building Blocks for Solid Phase Production of Diversity oriented Libraries. *Aust. J. Chem.* **2010**, *63*, 693–699.
- (24) Xiao, X. Y.; Li, R.; Zhuang, H.; Ewing, B.; Karunaratne, K.; Lillig, J.; Brown, R.; Nicolaou, K. C. Solid-phase combinatorial synthesis using MicroKan reactors, Rf tagging, and directed sorting. *Bio-technol. Bioeng.* **2000**, *71*, 44–50.
- (25) Dasgupta, P. Somatostatin analogues: multiple roles in cellular proliferation, neoplasia, and angiogenesis. *Pharmacol. Ther.* **2004**, *102*, 61–85.
- (26) Ferone, D.; Boschetti, M.; Resmini, E.; Giusti, M.; Albanese, V.; Goglia, U.; Albertelli, M.; Vera, L.; Bianchi, F.; Minuto, F. Neuroendocrine-immune interactions: the role of cortistatin/somatostatin system. *Ann. N.Y. Acad. Sci.* **2006**, *1069*, 129–144.
- (27) Tulipano, G.; Schulz, S. Novel insights in somatostatin receptor physiology. *Eur. J. Endocrinol.* **2007**, *156*, S3–S11.
- (28) Cervia, D.; Bagnoli, P. An update on somatostatin receptor signaling in native systems and new insights on their pathophysiology. *Pharmacol. Ther.* **2007**, *116*, 322–341.
- (29) Guillermet-Guibert, J.; Lahlou, H.; Cordelier, P.; Bousquet, C.; Pyronnet, S.; Susini, C. Physiology of somatostatin receptors. *J. Endocrinol. Invest.* **2005**, *28*, 5–9.
- (30) Barnett, P. Somatostatin and somatostatin receptor physiology. *Endocrine* **2003**, *20*, 255–264.
- (31) Pissios, P.; Bradley, R. L.; Maratos-Flier, E. Expanding the scales: The multiple roles of MCH in regulating energy balance and other biological functions. *Endocr. Rev.* **2006**, *27*, 606–620.
- (32) Wermter, A. K.; Reichwald, K.; Buch, T.; Geller, F.; Platzer, C.; Huse, K.; Hess, C.; Remschmidt, H.; Gudermann, T.; Preibisch, G.; Siegfried, W.; Goldschmidt, H. P.; Li, W. D.; Price, R. A.; Biebermann, H.; Krude, H.; Vollmert, C.; Wichmann, H. E.; Illig, T.; Sorensen, T. I.; Astrup, A.; Larsen, L. H.; Pedersen, O.; Eberle, D.; Clement, K.; Blundell, J.; Wabitsch, M.; Schafer, H.; Platzer, M.; Hieney, A.; Hebebrand, J. Mutation analysis of the MCHR1 gene in human obesity. *Eur. J. Endocrinol.* **2005**, *152*, 851–862.
- (33) Guesdon, B.; Paradis, E.; Samson, P.; Richard, D. Effects of intracerebroventricular and intra-accumbens melanin-concentrating hormone agonism on food intake and energy expenditure. *Am. J. Physiol. Regul. Integr. Comp. Physiol.* **2009**, *296*, R469–475.
- (34) Gehlert, D. R.; Rasmussen, K.; Shaw, J.; Li, X.; Ardayfio, P.; Craft, L.; Coskun, T.; Zhang, H. Y.; Chen, Y.; Witkin, J. M. Preclinical evaluation of melanin-concentrating hormone receptor 1 antagonism for the treatment of obesity and depression. *J. Pharmacol. Exp. Ther.* **2009**, *329*, 429–438.
- (35) Antal-Zimanyi, I.; Khawaja, X. The role of melanin-concentrating hormone in energy homeostasis and mood disorders. *J. Mol. Neurosci.* **2009**, *39*, 86–98.
- (36) Saito, Y.; Nagasaki, H. The melanin-concentrating hormone system and its physiological functions. *Results Probl. Cell Differ.* **2008**, *46*, 159–179.
- (37) Nahon, J. L. The melanocortins and melanin-concentrating hormone in the central regulation of feeding behavior and energy homeostasis. *C. R. Biol.* **2006**, *329*, 623–638; discussion 653–655.
- (38) Harrold, J. A.; Halford, J. C. The hypothalamus and obesity. *Recent Pat. CNS Drug Discovery* **2006**, *1*, 305–314.
- (39) McBriar, M. D. Melanin Concentrating Hormone Receptor Antagonists as Antiobesity Agents: From M2 to MCHR-1. *Curr. Top. Med. Chem.* **2007**, *7*, 1440–1454.
- (40) Luthin, D. R. Anti-obesity effects of small molecule melanin-concentrating hormone receptor 1 (MCHR1) antagonists. *Life Sci.* **2007**, *81*, 423–440.
- (41) McBriar, M. D. Recent advances in the discovery of melanin-concentrating hormone receptor antagonists. *Curr. Opin. Drug Discovery Dev.* **2006**, *9*, 496–508.
- (42) Judd, A. S.; Souers, A. J.; Kym, P. R. Lead optimization of melanin concentrating hormone receptor 1 antagonists with low hERG channel activity. *Curr. Top. Med. Chem.* **2008**, *8*, 1152–1157.
- (43) Rivera, G.; Bocanegra-Garcia, V.; Galiano, S.; Cirauqui, N.; Ceras, J.; Perez, S.; Aldana, I.; Monge, A. Melanin-concentrating hormone receptor 1 antagonists: a new perspective for the pharmacologic treatment of obesity. *Curr. Med. Chem.* **2008**, *15*, 1025–1043.
- (44) Kym, P. R.; Judd, A. S.; Lynch, J. K.; Iyengar, R.; Vasudevan, A.; Souers, A. J. Lead optimization strategies and tactics applied to the discovery of melanin concentrating hormone receptor 1 antagonists. *Curr. Top. Med. Chem.* **2007**, *7*, 1471–1488.
- (45) Kowalski, T. J.; Sasikumar, T. Melanin-concentrating hormone receptor-1 antagonists as antiobesity therapeutics: current status. *BioDrugs* **2007**, *21*, 311–321.
- (46) MacNeil, D. J.; Bednarek, M. A. MCH receptor peptide agonists and antagonists. *Peptides* **2009**, *30*, 2008–2013.